Near-field light emission from nano- and micrometric complex structures

M. Pieruccini[a)]
CNR, Istituto per i Processi Chimico-Fisici Sez. Messina, Via La Farina 237, I-98123 Messina, Italy

S. Savasta and R. Girlanda
Istituto Nazionale per la Fisica della Materia (INFM) and Dipartimento di Fisica della Materia e Tecnologie Fisiche Avanzate, Università di Messina Salita Sperone 31, I-98166 Messina, Italy

R. C. Iotti and F. Rossi
Istituto Nazionale per la Fisica della Materia (INFM) and Dipartimento di Fisica, Politecnico di Torino, Corso Duca degli Abruzzi 24, 10129 Torino, Italy

We propose a general theoretical scheme for the investigation of light emitted from nano- and micrometric structures of arbitrary shape and composition. More specifically, the proposed fully three-dimensional approach allows to derive the light-intensity distributions around the emitting structures and their modifications in the presence of nearby scattering objects. Our analysis allows to better identify the nontrivial relationship between near-field images and fluorescent objects. [DOI: 10.1063/1.1608483]

Recent continuous progress in scanning near-field microscopy together with the development of adequate nanofabrication techniques has enhanced our insight into the field distributions in the proximity of nano- and microstructured materials. This insight is of great relevance for the design of future optical circuitry able to process light with the versatility of electronic chips. These developments have stimulated more refined theoretical approaches as well as simulation strategies for the analysis of light propagation in complex structures and have renewed the interest in the classical theory of light scattering.[1,2] Indeed, theoretical predictions are essential for the design of photonic structures able to control the propagation of light. As a matter of fact, most of the theoretical investigations performed so far focus on the scattering of incident light illuminating structures of nontrivial shapes[1,3] or study light modes in photonic crystals and microcavities.[4] However, optical circuitry, besides passive elements controlling/manipulating the flow of photons, require active components able to emit and/or amplify light. This, in turn, opens relevant questions concerning the emission patterns of active mesoscopic systems: Which is the actual field distribution around emitting structures? How does the interaction with nearby scattering objects modify the field distribution? What kind of relationship between near-field images and fluorescent objects holds?

The aim of this letter is to provide a general theoretical framework for the evaluation of the field distributions in the proximity of three-dimensional (3D) mesoscopic fluorescent objects in the presence of nearby scattering structures. The proposed quantum theory of light emission can be applied to a great variety of nanostructured optically active materials as mesoscopic dielectric objects uniformly doped with optically active molecules (e.g., dye molecules) or embedding semiconductor dots or layers able to emit light when appropriately excited.

As a starting point, let us consider the key quantity we want to investigate, i.e., the spectrally resolved energy density $\mathcal{I}(\mathbf{r},\omega)$ corresponding to the electric field at point $\mathbf{r}$; this can be defined as:

$$\frac{\varepsilon_0}{2}\langle \hat{\mathbf{E}}^-(\mathbf{r},\omega)\cdot\hat{\mathbf{E}}^+(\mathbf{r},\omega')\rangle = \mathcal{I}(\mathbf{r},\omega)\,\delta(\omega-\omega'), \tag{1}$$

where $\hat{\mathbf{E}}^+(\mathbf{r},\omega)$ is the electric-field operator corresponding to the positive frequency ω (it can be expanded in terms of photon destruction operators) and $\hat{\mathbf{E}}^-(\mathbf{r},\omega)$ is its Hermitian conjugate. Our theoretical approach is based on the Green's tensor technique in the frequency domain.[1,5] The electric field operator at a given positive frequency can be regarded as the sum of scattering and emission contributions:[5] $\hat{\mathbf{E}}^+(\mathbf{r},\omega)=\hat{\mathbf{E}}_s^+(\mathbf{r},\omega)+\hat{\mathbf{E}}_e^+(\mathbf{r},\omega)$. The first term describes light coming from free-space and scattered by the material system, i.e.,

$$\hat{\mathbf{E}}_s^+(\mathbf{r},\omega)=\hat{\mathbf{E}}_0^+(\mathbf{r},\omega) - k^2\int \vec{\mathbf{G}}(\mathbf{r},\mathbf{r}',\omega)\chi(\mathbf{r}',\omega)\hat{\mathbf{E}}_0^+(\mathbf{r}',\omega)\,d\mathbf{r}', \tag{2}$$

where $k=\omega/c$, the free-space electric-field operator $\hat{\mathbf{E}}_0^+$ describes input light, and $\chi=\varepsilon-1$ is the susceptibility function of the material system (that we have assumed to be a local and scalar function to avoid complications), and $\vec{\mathbf{G}}$ is the field Green tensor.[1,5] We stress that nonlocality and/or anisotropy can also be implemented.[5] The second term $\hat{\mathbf{E}}_e^+$ describes light emitted by the material system itself, i.e.,

$$\hat{\mathbf{E}}_e^+(\mathbf{r},\omega) = -i\omega\mu_0\int \vec{\mathbf{G}}(\mathbf{r},\mathbf{r}',\omega)\hat{\mathbf{j}}(\mathbf{r}',\omega)\,d\mathbf{r}', \tag{3}$$

where the integration is performed over the volume of the scattering system and μ_0 denotes the magnetic permeability of vacuum. Here, the quantum noise operators $\hat{\mathbf{j}}$ are the sources of spontaneous light emission. These zero-mean operators can be derived from the Heisenberg–Langevin equations for the material system[6] and are present only if the

a)Electronic mail: pieruccini@me.cnr.it

susceptibility tensor describing the material system has an imaginary part; they are a direct consequence of the fluctuation–dissipation theorem.

It is easy to verify that the intensity of the emitted light $\langle \hat{\mathbf{E}}_e \hat{\mathbf{E}}_e^{+} \rangle$ is directly related to the correlation function of quantum noise currents: $\langle \hat{\mathbf{j}}^{\dagger} \cdot \hat{\mathbf{j}} \rangle$. In order to calculate it explicitly we adopt a simple two-level molecular model to describe the dielectric function of the scattering system,

$$\chi(\mathbf{r},\omega) = \chi_s(\mathbf{r}) + \frac{\mathcal{N}(\mathbf{r}) e^2 f_{ab}}{m\varepsilon_0} \frac{N_a(\mathbf{r}) - N_b(\mathbf{r})}{\omega_0 - \omega + i\gamma}, \tag{4}$$

where χ_s is the real susceptibility of the scattering system in the absence of active molecules, f_{ab} is the oscillator strength associated to the transition [related to the associate dipole moment d by $f_{ab} = 2\omega_0 m d^2/(\hbar e^2)$], $\mathcal{N}$ gives the density of active molecules, and $N_{a(b)}$ indicates the population densities of the (a) upper and (b) lower levels. This simple model can be easily extended to include non-random molecular orientations, more energy levels and molecular species. Also more complex models describing, e.g., semiconductor dielectric functions,[6] can be adopted. By adopting this model and following Ref. 5, we obtain

$$\langle \hat{j}_l^{\dagger}(\mathbf{r},\omega) \hat{j}_{l'}(\mathbf{r}',\omega') \rangle = \frac{\hbar}{\pi\mu_0} \frac{\omega^2}{c^2} \mathrm{Im}[\chi(\mathbf{r},\omega)] \times N(\mathbf{r}) \delta_{ll'} \delta(\mathbf{r}-\mathbf{r}') \delta(\omega-\omega'), \tag{5}$$

with the population factor $N(\mathbf{r}) = N_a(\mathbf{r})/[N_b(\mathbf{r}) - N_a(\mathbf{r})]$. Presently, our main interest is the case where input photons are absent [i.e., $\langle \mathbf{E}_0^{-}(\mathbf{r},\omega) \cdot \mathbf{E}_0^{+}(\mathbf{r},\omega') \rangle = 0$]. In this case we obtain $\mathcal{I}(\mathbf{r},\omega) = \Sigma_l \mathcal{I}_l(\mathbf{r},\omega)$ with

$$\mathcal{I}_l(\mathbf{r},\omega) = \frac{\hbar k^4}{2\pi} \sum_{l'} \int N(\mathbf{r}') \varepsilon^I(\mathbf{r}',\omega) |G_{ll'}(\mathbf{r},\mathbf{r}',\omega)|^2 d\mathbf{r}'. \tag{6}$$

We observe that population densities in principle are affected by light emission, thus Eq. (6) should be solved self-consistently together with the rate equations for the populations. However, in many cases (far from the laser threshold), population densities are poorly affected by light emission and propagation, being fixed by external pumping. We also observe that Eq. (6) has a structure analogous to the corresponding equation describing emission from thermal sources.[7,8]

To assess the power and versatility of the proposed scheme, we investigate the field-intensity distribution around a fluorescent low-symmetry nanostructured system. We consider an overall emitting 3D object consisting of a pair of quavers. The pad on the right is made of silver,[9] and the rest of the structure has relative dielectric constant of $\varepsilon = 4 + 0.2i$ with the exception of a small bleached square on the top region [see outline in Fig. 1(a)] with dielectric function $\varepsilon = 4$. The adopted value of the imaginary part of the dielectric function is typical for organic dye molecules distributed with quite high density.[10] In particular [see Eq. (4)], $\mathrm{Im}\,\chi^I = 0.2$ corresponds, e.g., to a distribution of active molecules with density $\mathcal{N}^{-1} \simeq 10\ \mathrm{nm}^3$, oscillator strength $f_{ab} = 0.03$ at detuning $(\omega_0 - \omega)/\omega_0 = 0.02$, ($\omega$ is the emission frequency). The whole structure has a uniform thickness of 60 nm, an extension in the other two dimensions of about 450 $\times$ 380 nm and lies on a flat substrate of uniform dielectric constant of $\varepsilon_s = 2.5$. In principle the emitting system can be excited by current injection or by optical excitation at frequencies higher than the emission frequency. In order to better focus on the emission properties, in the following we assume uniform excitation leading to uniform population densities. The effect of nonuniform excitation at higher energies by far-field illumination can also be taken into account within the present approach. In this case the population factor $N(\mathbf{r})$ will be proportional (in the linear regime) to $\varepsilon^I(\mathbf{r},\omega_e)|E_s(\mathbf{r},\omega_e)|^2$, where $\mathbf{E}_s$ is the field originating from far-field illumination [see Eq. (2)], and ω_e is the excitation frequency. Figure 1(a) displays $\mathcal{I}(x,y,\overline{z},\omega)$ in the proximity of the emitting object in an observation plane located at $\overline{z} = 52.5$ nm above the top surface of the structure (i.e., 112.5 nm above the substrate). The Green tensor is computed by solving numerically a discretization of the Dyson equation.[1] Calculations have been made at $\lambda = 2\pi c/\omega = 600$ nm. The emission pattern reproduces almost perfectly the object shape and both the bleached region and the metallic pad can be clearly distinguished. The vector character of the emitted light is shown in Figs. 1(b)–1(d), where the partial intensities $\mathcal{I}_l(\mathbf{r},\omega)$ (i.e., the intensities that can be detected by a probe able to select light polarization) are displayed. In spite of the isotropic and uncorrelated character of the source currents, the three intensity distributions strongly differ one from each other. We observe that only $\mathcal{I}_z$ reproduces quite well the object shape (except the metallic pad of course). Besides, from inspection of Figs. 1(a) and 1(d), a rather complex intensity pattern can be observed around the metallic pad. This nonuniform pattern, mainly polarized along the z axis, can be attributed to the excitation of multipolar modes by the incoherent light originating from the nearby fluorescent structure.[11]

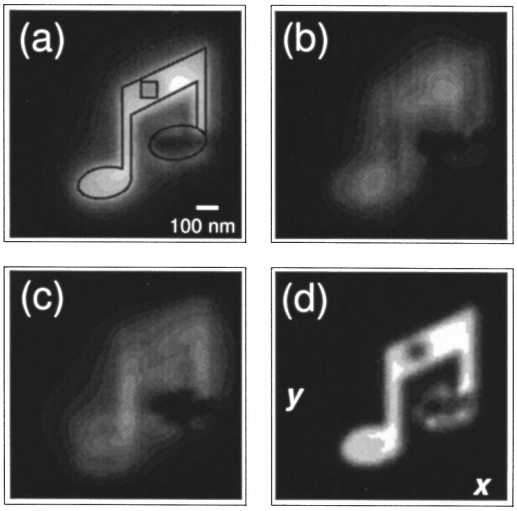

FIG. 1. (a) Overall field intensity $\mathcal{I}(\mathbf{r},\omega)$, in an observation plane 112.5 nm above the substrate, emitted at $\lambda = 600$ nm from the structure, and partial intensities $\mathcal{I}_l(\mathbf{r},\omega)$: (b) $\mathcal{I}_x$, (c) $\mathcal{I}_y$, (d) $\mathcal{I}_z$. The same intensity range has been chosen for the representation of the last three panels (so that a given brightness matches the same intensity for all). The intensity interval of the first panel has been duly compressed for clarity of the figure.

Figure 2 shows the differences in contrast, resolution, and light confinement between fluorescence and scattering near-field patterns. The latter has been obtained with a

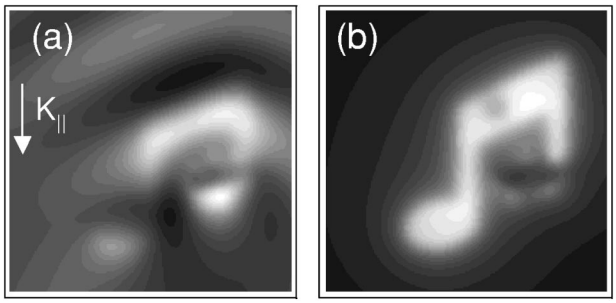

FIG. 2. (a) Intensity amplitude $|\mathbf{E}_s|^2$ in the same observation plane of Fig. 1, and at the same wavelength, resulting from illumination by a *p*-polarized plane wave at $\pi/4$ incidence (the projection of the incident wave vector on the *xy* plane, $k_{\|}$, is also indicated). The dielectric and geometric features of the structure are reported in the text (see also Fig. 1). (b) The field-intensity distribution emitted (fluorescence) by the same structure [see also Fig. 1(a), where the structure is outlined].

p-polarization excitation incident at $\pi/4$ from above the substrate. Besides the fact that scattering completely ignores the bleached region, we observe that the two panels display very different (almost complementary) behaviors as to what concerns contrast, resolution, and light confinement. In particular, a rather widely spreadout light pattern around the dielectric structure appears to be inherent to the scattering configuration. Moreover, note (i) the interference pattern in the top region of Fig. 2(a), which may at first appear as a ghost structure, and (ii) the apparent shift of the object along the projection on the *xy* plane of the incident wave vector (the position of the quavers relative to the frame is the same in both cases). We also observe that the two different excitation mechanisms of the metallic pad (i.e., incoherent nearby emission field or coherent far-field illumination) induce rather different intensity patterns around it. The differences here observed between scattering and emission patterns in part can be led to the fact that fluorescence is an intrinsically incoherent process in contrast with scattering. In particular Eq. (6) shows that the emitted field amplitude from individual emitters is first squared and then summed up, whereas scattered light intensity [see Eq. (2)] is obtained by the reversed procedure.

We have proposed a general theoretical scheme for the investigation of light emitted from nano- and micrometric structures of arbitrary shape and composition. We showed that the shape of the object is relevant in the polarization properties of the emission pattern. In particular we have found an enhancement of the *z* component of the field emitted by incoherent, nonpolarized sources distributed substantially in the *xy* plane. The presented numerical results provide useful guidelines for the interpretation of near-field photoluminescence spectroscopy/microscopy measurements. Moreover this theoretical and numerical scheme can be applied to the design of photonic systems combining active and passive structures.

The authors thank Omar Di Stefano for stimulating discussions.

[1] O. J. F. Martin, C. Girard, and A. Dereux, Phys. Rev. Lett. **74**, 526 (1995).
[2] A. Madrazo and M. Nieto-Vesperinas, Appl. Phys. Lett. **70**, 31 (1997).
[3] S. Fan, I. Appelbaum, and J. D. Joannopoulos, Appl. Phys. Lett. **75**, 3461 (1999).
[4] J. D. Joannopoulos, R. D. Meade, and J. N. Winn, *Photonic Crystals* (Princeton University Press, Princeton, NJ, 1995).
[5] S. Savasta, O. Di Stefano, and R. Girlanda, Phys. Rev. A **65**, 043801 (2002).
[6] C. H. Henry and R. F. Kazarinov, Rev. Mod. Phys. **68**, 801 (1996).
[7] J. P. Mulet, K. Joulain, R. Carminati, and J.-J. Greffet, Appl. Phys. Lett. **82**, 1660 (1999).
[8] J.-J. Greffet, R. Carminati, K. Joulain, J. P. Mulet, S. P. Mainguy, and Y. Chen, Nature (London) **416**, 6876 (2002).
[9] The dielectric function of silver was obtained interpolating the values obtained by P. B. Johnson and R. W. Christy, Phys. Rev. B **6**, 4370 (1972).
[10] I. Pockrand, J. D. Swalen, R. Santo, A. Brillante, and M. R. Philpott, J. Chem. Phys. **69**, 4001 (1978).
[11] Experimental evidence of quadrupolar plasmon patterns at about these wavelengths has been recently reported by R. Hillenbrand and F. Keilmann, Appl. Phys. B: Lasers Opt. **73**, 239 (2001).